MICROBIOLOGY

Inverse control of Rab proteins by *Yersinia* ADP-ribosyltransferase and glycosyltransferase related to clostridial glucosylating toxins

G. Stefan Ost[1,2], Christophe Wirth[3], Xenia Bogdanović[3], Wei-Chun Kao[3], Björn Schorch[1], Philipp J. K. Aktories[1], Panagiotis Papatheodorou[1], Carsten Schwan[1], Andreas Schlosser[4], Thomas Jank[1]*, Carola Hunte[3,5,6], Klaus Aktories[1,5†]

We identified a glucosyltransferase (YGT) and an ADP-ribosyltransferase (YART) in *Yersinia mollaretii*, highly related to glucosylating toxins from *Clostridium difficile*, the cause of antibiotics-associated enterocolitis. Both *Yersinia* toxins consist of an amino-terminal enzyme domain, an autoprotease domain activated by inositol hexakisphosphate, and a carboxyl-terminal translocation domain. YGT *N*-acetylglucosaminylates Rab5 and Rab31 at Thr^{52} and Thr^{36}, respectively, thereby inactivating the Rab proteins. YART ADP-ribosylates Rab5 and Rab31 at Gln^{79} and Gln^{64}, respectively. This activates Rab proteins by inhibiting GTP hydrolysis. We determined the crystal structure of the glycosyltransferase domain of YGT (YGT^{G}) in the presence and absence of UDP at 1.9- and 3.4-Å resolution, respectively. Thereby, we identified a previously unknown potassium ion–binding site, which explains potassium ion–dependent enhanced glycosyltransferase activity in clostridial and related toxins. Our findings exhibit a novel type of inverse regulation of Rab proteins by toxins and provide new insights into the structure-function relationship of glycosyltransferase toxins.

INTRODUCTION

Large clostridial glucosylating toxins (CGTs) are major virulence factors and play pivotal roles in many diseases. Prototypes of these exotoxins are toxins A (TcdA) and B (TcdB) of *Clostridium* (*Clostridioides*) *difficile*, which are responsible for antibiotics-associated diarrhea and pseudomembranous colitis (*1*, *2*). TcdA and TcdB are multidomain toxins and consist of an N-terminal glucosyltransferase domain, an autoprocessing cysteine protease domain, a translocation domain, and a C-terminal region called CROPs (combined repetitive oligopeptides) involved in receptor binding (*1*). After binding, the receptor-toxin complex is endocytosed to reach acidic endosomal compartments from where the toxins (or parts of the toxins) translocate into the cytosol (*3*). Here, the cysteine protease domain is activated by inositol hexakisphosphate ($InsP_6$), resulting in cleavage of the toxin and release of the glucosyltransferase domain into the cytosol (*4*, *5*). Subsequently, the glucosyltransferase glucosylates Rho proteins at Thr^{37} (e.g., RhoA, RhoB, and RhoC) or Thr^{35} of Rac and Cdc42; thereby, the functions of Rho proteins are inhibited (*6*). Various clostridial toxins share the molecular architecture of TcdA and TcdB, including lethal toxin and hemorrhagic toxins of *Clostridium sordellii* and the α-toxin of *Clostridium novyi* (*1*). The *Clostridium perfringens* toxin TpeL is another member of this toxin family, which GlcNAcylates Ras and Rac proteins (*7*). TpeL differs from other toxins because it has no CROP domain.

Yersinia are Gram-negative bacteria. The genus *Yersinia* has at least 18 species. Only three are known as major human pathogens, including *Yersinia pestis*, *Yersinia enterocolitica*, and *Yersinia pseudotuberculosis*. The pathogens produce numerous virulence factors (*8*). Well studied are various *Yersinia* surface adhesins (e.g., YadA, Ail, and Psa) and the large group of *Yersinia* outer proteins, which are delivered into host cells by type III secretion (*8*). Another well-characterized pathogen is *Yersinia ruckeri*, a fish pathogen, which causes the enteric red mouth disease in salmonid fish (*9*). Recently, AFP18, which is an effector of the type VI secretion-like antifeeding prophage (AFP) complex of *Y. ruckeri*, has been identified as a tyrosine glycosylating virulence factor (*10*). Here, we report on two previously unknown toxins produced by *Yersinia mollaretii*, which largely share the same multidomain architecture with CGTs. While one toxin is a glycosyltransferase, the other toxin has adenosine diphosphate (ADP)–ribosyltransferase activity. Unexpectedly, we found that the substrates of the toxins are Rab proteins, which are bidirectionally (inversely) regulated by the toxins.

RESULTS

C. difficile toxin–related proteins in *Y. mollaretii*

By comparing the protein sequence of *C. difficile* toxin B (TcdB) with protein sequences of the genus *Yersinia*, two *Y. mollaretii* proteins were found, which shared substantial similarities with TcdB (Fig. 1A). One protein (WP_004876989.1) exhibited similarity with TcdB over the entire protein sequence until amino acid 1834 of TcdB. This protein was called YGT (*Yersinia* glycosyltransferase). Sequence analysis revealed an N-terminal enzyme domain, followed by a cysteine protease domain and a C-terminal translocation and binding domain with TcdB. However, like in *C. perfringens* TpeL, the C-terminal CROP domain of TcdB was missing in YGT (fig. S1) (*7*). The second *Yersinia* protein (WP_004874725.1) largely differed in its N terminus from YGT and TcdB but shared sequence similarities

[1]Institut für Experimentelle und Klinische Pharmakologie und Toxikologie, Medizinische Fakultät, Albert-Ludwigs-Universität Freiburg, 79104 Freiburg, Germany. [2]Institut für Biologie, Fakultät für Biologie, Albert-Ludwigs-Universität Freiburg, 79104 Freiburg, Germany. [3]Institut für Biochemie und Molekularbiologie, ZBMZ, Medizinische Fakultät, Albert-Ludwigs-Universität Freiburg, 79104 Freiburg, Germany. [4]Rudolf-Virchow-Zentrum für Experimentelle Biomedizin, Universität Würzburg, 97080 Würzburg, Germany. [5]Centre for Biological Signalling Studies (BIOSS), Albert-Ludwigs-Universität Freiburg, 79104 Freiburg, Germany. [6]CIBSS–Centre for Integrative Biological Signalling Studies, University of Freiburg, 79104 Freiburg, Germany.
*Present address: Pfizer Manufacturing Deutschland GmbH, 79090 Freiburg, Germany.
†Corresponding author. Email: klaus.aktories@pharmakol.uni-freiburg.de

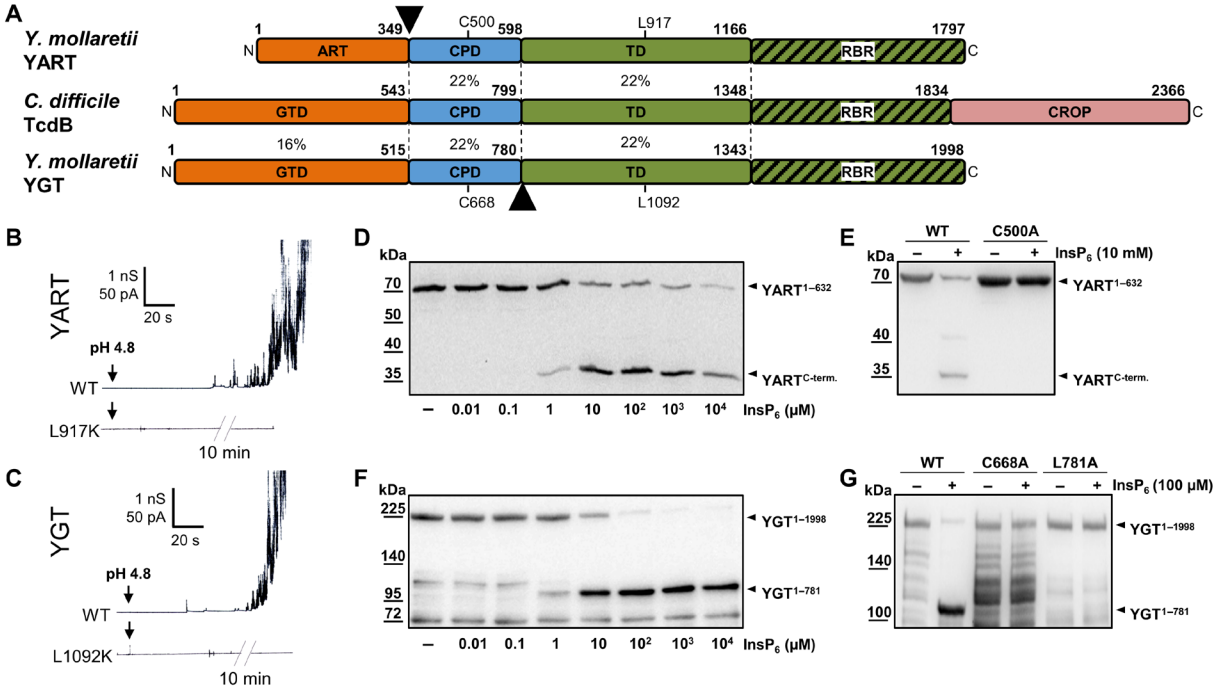

Fig. 1. Domain architecture of YART and YGT and analysis of the translocation and protease domains. (**A**) Domain comparison of YART, TcdB, and YGT. The N-terminal domain of YART is an ADP-ribosyltransferase (ART), whereas the N terminus of YGT and TcdB harbors glycosyltransferases (GTD). Like TcdB, YART and YGT have an autocatalytic cysteine protease domain (CPD) and a translocation domain (TD). The C terminus of the TD of TcdB contains a receptor-binding region (RBR). Only TcdB has a CROP domain. Sequence identities of regions indicated by amino acid numbers are in percentage. Arrowheads mark split products of YART and YGT. Cys^{500} and Leu^{917} of YART and Cys^{668} and Leu^{1092} of YGT indicate the essential cysteine of CPDs and the critical leucine of TDs. (**B** and **C**) Membrane activity in lipid bilayer by YART, YGT, and their mutants YART L917K and YGT L1092K. Pore formation was induced by acidification to pH 4.5. The mutants did not induce increase in electric conductance, even after prolonged incubation (10 min). (**D** and **F**) In vitro processing of $YART^{1–632}$ and $YGT^{1–1998}$ at the indicated concentrations of $InsP_6$, resulting in fragments $YART^{C\text{-}term}$ and $YGT^{1–781}$. (**E** and **G**) Inhibition of autocatalytic cleavage in mutants $YGT^{1–1998}$ L781A, $YGT^{1–1998}$ C668A, and $YART^{1–632}$ C500A in the presence of $InsP_6$. Western blots with anti-His antibody are shown. WT, wild type.

in the middle and C-terminal parts of the protein with CGTs. This toxin exhibited N-terminal sequence similarity with ADP-ribosyltransferases (see below) and was designated as YART (*Yersinia* ADP-ribosyltransferase).

Membrane activity in lipid bilayer

Pore formation is likely involved in translocation of TcdB and related toxins (*3*, *11*). We studied pore formation of the *Yersinia* toxins in lipid bilayer by monitoring the increase in electric conductance upon acidification of the medium from pH 7.5 to <6 (Fig. 1, B and C) (*3*). After acidification, YGT and YART exhibited enhanced membrane activity and increased the electrical conductance of lipid membranes but did not induce a defined stepwise increase in conductance. A similar type of interaction with lipid membranes is known for TcdB (*3*). Notably, *Yersinia* toxins are highly similar to TcdB (and TcdA) in a peptide region around amino acids 1080 to 1093 of YGT and amino acids 905 to 918 of YART (fig. S1C). This region is essential for translocation of TcdB and is conserved in all CGTs (*11*). In TcdB, change of Leu^{1106} to lysine causes inhibition of toxin-induced pore formation (*11*). Similarly, we observed an inhibition of increased membrane activity with the mutations L917K and L1092K of YART and YGT, respectively (Fig. 1, B and C). These findings suggest highly related translocation mechanisms of the *Yersinia* toxins as compared with TcdB.

Autoproteolytic activities of YGT and YART

CGTs share an autocatalytic cysteine protease domain, which is allosterically activated by $InsP_6$ (*4*, *5*). Similarly, the autoproteolytic activities of YGT and YART were activated by $InsP_6$ (Fig. 1, D and F). As in all clostridial glucosyltransferase toxins, the cleavage of YART occurred between the cysteine protease domain and the proposed N-terminal enzyme domain (Fig. 1D) (*4*, *5*). Figure 1D shows the $InsP_6$-induced cleavage of the N-terminal YART fragment (amino acids 1 to 632), containing the N-terminal enzyme domain and the proposed upstream protease domain with an additional His tag. This fragment was used because the complete toxin exhibited additional protein bands after purification (fig. S2A), while this was not the case with the N-terminal fragment. Autocleavage in the presence of 1 to 10 μM $InsP_6$ released a ~30-kDa C-terminal peptide. The autoprotease activity of CGTs depends on a catalytic aspartate, histidine, and cysteine (DHC) triad (*4*), which is conserved in the proposed protease domain of YART with Asp^{392}, His^{454}, and Cys^{500}. As shown in Fig. 1E, YART C500A did not exhibit autocleavage activity in the presence of $InsP_6$ (10 mM).

For cleavage studies with YGT, we used the full-length toxin of ~230 kDa, carrying a His and Sumo tag at the N terminus, which largely increased the expression yield. Unexpectedly, in the presence of $InsP_6$, cleavage of YGT occurred downstream of the autocatalytic cysteine protease domain, releasing a fragment of ~110 kDa (Fig. 1F).

Accordingly, we did not detect any additional split product, when a toxin fragment, covering the N-terminal enzyme domain and the protease domain only (amino acids 1 to 760), was used (fig. S2B). Sequence analysis suggested that in YGT, cleavage was most likely behind Leu^{781}. This hypothesis was supported by mass spectrometric (MS) analysis. Moreover, when Leu^{781} of YGT was changed to alanine, cleavage was prevented (Fig. 1G). As found for the protease domain of YART, exchange of the highly conserved cysteine residue (Cys^{668}) of the proposed catalytic triad (Asp^{562}, His^{625}, and Cys^{668}) of YGT resulted in inhibition of autocleavage (Fig. 1G).

Enzyme activity of YART

While the N-terminal region of YART did not exhibit substantial amino acid sequence similarity with CGTs (fig. S1B), we recognized similarity with ADP-ribosyltransferases from the R-S-E type like cholera and pertussis toxins (Fig. 2A) (*12*).

We expressed the ADP-ribosyltransferase domain of YART (amino acids 1 to 349; henceforth called YART^{A}) in *Saccharomyces cerevisiae* under the control of a galactose-dependent promoter (Fig. 2B). This resulted in moderate growth inhibition of yeast, when galactose was present. Sequence alignment suggested that Glu^{160} of YART was the so-called catalytic glutamate, which is conserved in all ADP-ribosyltransferases and essential for enzyme activity (*12*). Accordingly, expression of YART^{A} E160A (verified by Western blot; fig. S2C) did not affect yeast growth, supporting the view that YART acts as an ADP-ribosyltransferase. Next, we ADP-ribosylated yeast cell lysate with YART^{A} in the presence of [^{32}P]NAD^{+} (nicotinamide adenine dinucleotide). This resulted in radioactive labeling of ~25-, ~35-, and ~40-kDa proteins (fig. S2D). Labeling of the 40-kDa protein band was obviously caused by auto–ADP-ribosylation. MS analysis of the heavily labeled 25-kDa protein band revealed various YPT proteins, including YPT1, YPT6, YPT7,

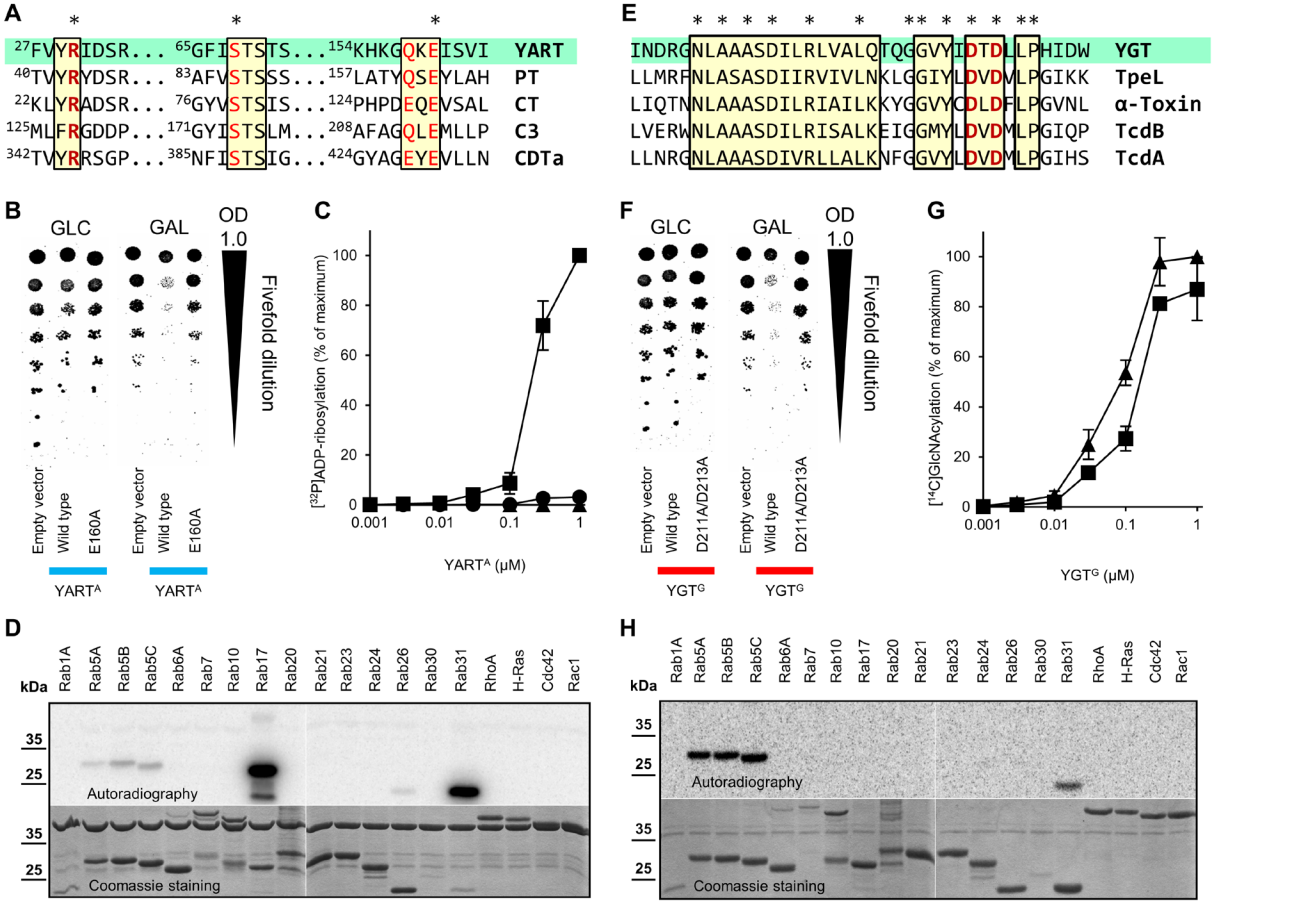

Fig. 2. ADP-ribosylation by YART and glycosylation by YGT. (**A**) Sequence comparison of ADP-ribosyltransferases [YART, pertussis toxin (PT; P04977), cholera toxin (CT; P01555), *Clostridium botulinum* C3 toxin (C3; P15879), and *C. difficile* ADP-ribosyltransferase (CDTa; Q9KH42)]. Conserved amino acids are marked in red; R-S-E amino acid motifs are indicated by asterisk. (**B**) Spot test of *S. cerevisiae* growth. Yeast cells, expressing YART^{A} or mutants under control of a galactose-dependent promoter, were spotted on glucose (GLC) and galactose (GAL) plates in fivefold dilutions. OD, optical density. (**C**) ADP-ribosylation of Rab proteins. Rab5A (▲), Rab31 (■), and Rab17 (●) (each 5 μg) were incubated at the indicated concentrations of YART^{A} with 1 μM [^{32}P]NAD^{+} for 15 min, followed by SDS–polyacrylamide gel electrophoresis (PAGE) and phosphorimaging (data are means ± SD; $n = 3$). (**D**) Substrates of YART. Indicated guanosine triphosphatases (GTPases) (Rab31, 0.2 μg; other, 2 μg) were incubated with YART^{A} (3 μM) and [^{32}P]NAD^{+} as in (C). Coomassie staining and autoradiogram are shown. (**E**) Sequence alignment of the DXD region of glucosyltransferase toxins [YGT, *C. perfringens* TpeL (A2PYQ6), *C. novyi* α-toxin (Q46149), and *C. difficile* TcdB (P18177) and TcdA (P16154)]. (**F**) Growth spot test of YGT^{G} or mutants in yeast cells as in (B). (**G**) Glycosylation of Rab5A (▲)and Rab31 (■) (each 5 μg) with YGT^{G} and UDP-[^{14}C]GlcNAc (10 μM) for 15 min. Analysis of labeled proteins as in (C). (**H**) Substrates of YGT. Indicated GTPases (each 2 μg) were incubated with YGT^{G} (0.5 μM) and UDP-[^{14}C]GlcNAc as in (G).

YPT32, YPT11, YPT31, YPT8, and SEC4, but not a direct attachment of ADP-ribose. Because YPT proteins are orthologs of Rab proteins, we tested the ADP-ribosylation of Rab, Rho, and Ras proteins in vitro (Fig. 2D). These studies revealed ADP-ribosylation of Rab31, Rab17, and Rab5 by YART^{A}. In contrast, Rho proteins (RhoA, Rac, and Cdc42) and H-Ras proteins were not modified. Further analysis of the kinetics of YART^{A}-induced ADP-ribosylation showed that Rab31 was the preferred substrate of the *Yersinia* enzyme in vitro (Fig. 2C), showing a >50-fold higher rate in ADP-ribosylation of Rab31 than of Rab17, while Rab5 was only marginally modified under these conditions (low NAD concentration of 1 μM).

Enzyme activity of YGT

The N-terminal part of YGT exhibited substantial sequence similarity with CGTs (Fig. 2E and fig. S1B). Therefore, we studied whether YGT had glycohydrolase activity, a typical property of many glycosyltransferase toxins (*13*). When radiolabeled uridine diphosphate (UDP)–glucose or UDP–*N*-acetylglucosamine (GlcNAc) was incubated with the N-terminal domain of YGT (amino acids 1 to 520; henceforth called YGT^{G}), hydrolysis of UDP-GlcNAc but not of UDP-glucose was detected, suggesting that UDP-GlcNAc was the preferred sugar donor (fig. S2E). As for TcdB, the glycohydrolase activity of YGT^{G} depended on the presence of Mn^{2+} or Mg^{2+} (fig. S2F).

As found for YART^{A}, expression of YGT^{G} in *S. cerevisiae* inhibited yeast growth (Fig. 2F). Growth inhibition was prevented by mutation of the DXD motif (YGT^{G} D211A/D213A), which plays a pivotal role in many glycosyltransferases (*13*–*15*). Next, we studied the GlcNAcylation of small guanosine triphosphatases (GTPases) by YGT^{G} in vitro (Fig. 2H), showing that Rab5 and Rab31 were strongly modified by YGT^{G}. By contrast, Rho or Ras proteins, which are the preferred substrates of CGTs like TcdB, were not modified. The concentration-effect curve of YGT-induced GlcNAcylation exhibited a slight preference for Rab5 (Fig. 2G).

Crystal structure analysis of YGT

To gain insights into the architecture and mechanism of the glycosyltransferase domain of YGT, we determined its x-ray structure. A His-tagged construct of YGT^{G} was produced by heterologous expression, purified by affinity chromatography, and the affinity tag was removed by TEV (tobacco etch virus)–protease cleavage. Crystals were obtained in the absence of ligands as well as in the presence of UDP and $MnCl_2$. The structure of YGT^{G} with UDP and Mn^{2+} bound was solved using native SAD (single-wavelength anomalous diffraction), and it was refined to 1.9-Å resolution (table S1). The ligand-free structure was solved by molecular replacement and refined at 3.4-Å resolution (table S1).

YGT^{G} has a globular structure, which can be divided into two parts. N-terminally, a typical GT-A glycosyltransferase fold comprises a central seven-stranded, mixed β sheet surrounded by 16 α helices in a Rossmann fold–like arrangement (Fig. 3A and fig. S3A). The C-terminal end of the construct comprises a compact antiparallel five-helix bundle (Fig. 3A and fig. S3A). The N-terminal part of YGT^{G} displays high structural similarity with the core glycosyltransferase domain of various toxins. Highest homology was found for clostridial toxins including the lethal toxin from *C. sordellii* as well as toxins A and B from *C. difficile* (Fig. 3B and table S2) (*14*, *16*, *17*). The N-terminal four-helix bundle characteristic for clostridial glycosylating toxins is absent in YGT^{G}. Substantial homology is also present for the smaller glycosyltransferase domains of the PaTox toxin from *Photorhabdus asymbiotica* (*18*) and the *Salmonella* effectors SseK1 and SseK3 (*19*, *20*). The C-terminal five-helix bundle appears to be specific for YGT^{G} and has no equivalent counterpart in the identified structural homologs. The first helix of the bundle, however, superimposes well with the C-terminal helix of TcdB.

The 1.9-Å structure of YGT^{G} sheds light on the nucleotide-binding mode (Fig. 3, C to F). The uridine moiety is stabilized by an aromatic π stacking with Trp^{23} and by four hydrogen bonds, particularly with the backbone atoms of residues Trp^{23} and Ile^{24} (Fig. 3C). The ribose moiety is stabilized by several direct or water-mediated hydrogen bonds to either main- or side-chain atoms of Val^{22}, Ser^{194}, Tyr^{209}, and Thr^{212} (Fig. 3D). The side chains of Asp^{211} and Asp^{213}, namely, the conserved DXD motif and the adjacent manganese ion (Mn^{2+}), are central for the coordination of the diphosphate moiety (Fig. 3E). The nature of the metal ion was confirmed using the anomalous signal of manganese at 6.7 keV (data not shown). The side chain of Asp^{213} and one oxygen atom of each α and β-phosphate directly coordinate the Mn^{2+}. Asp^{211} contributes a water-mediated interaction. The typical octahedral coordination of Mn^{2+} is completed with a water molecule and with the side chain of Glu^{427} from helix 17 (Fig. 3E). The side-chain oxygen atom of Asp^{213} is coordinating not only Mn^{2+} but also a second atom that was showing a strong peak in the native SAD anomalous Fourier electron density map (fig. S3B). The atom was assigned as potassium ion. It is further coordinated by the main-chain carbonyl groups of residues Glu^{426} and Phe^{429} and by the α-phosphate moiety of UDP as well as by several water molecules including one belonging to the first coordination sphere of Mn^{2+} (Fig. 3, E and F, and fig. S3B). It is well established that the glycohydrolase and glucosyltransferase activities of CGTs are increased by potassium but not by sodium ions (*21*–*23*). Similarly, the glycosyltransferase activity of YGT was enhanced by potassium ions (fig. S3C).

Notably, the C terminus of the glycosyltransferase domain comprising the short helix 17 and its consecutive loop (residues Phe^{429} to Tyr^{438}) encloses the nucleotide-binding site as a lid with multiple interactions to the diphosphate (Ser^{430} and Trp^{432} to β-phosphate and Ser^{431} to α-phosphate) (Fig. 3F). In the ligand-free YGT^{G} structure, which is overall highly similar to the UDP-bound state (1.4-Å root mean square deviation for all atoms), the aforementioned lid is shifted by about 8 Å, including a reorientation of the conserved Trp^{432} side chain resulting in an open ligand-binding site (fig. S4).

Rab modification by YART and YGT

Next, modification of Rab31 and Rab5 by YART and YGT was analyzed by MS (fig. S5, A to C). These analyses revealed that YART^{A} ADP-ribosylated Rab31 at Gln^{64} and Rab5 at the equivalent Gln^{79}, whereas YGT^{G} transferred GlcNAc to Rab5 in position Thr^{52} (Fig. 4A and fig. S6A). YGT^{G}- and YART^{A}-induced modifications of Rab proteins were verified by site-directed mutagenesis of Rab5 and Rab31 (Fig. 4B and fig. S6B). The mutant protein Rab5A T52A was not GlcNAcylated by YGT^{G} but slightly ADP-ribosylated by YART^{A}. On the other hand, the mutant protein Rab5A Q79L was not ADP-ribosylated by YART^{A} but GlcNAcylated by YGT^{G}. Similar results were obtained with Rab31. YART was not capable to ADP-ribosylate Rab31 Q64L, while YGT caused GlcNAcylation of the mutant Rab31 protein, however, with reduced activity. As expected, GlcNAcylation was blocked in the mutant Rab31 T36A.

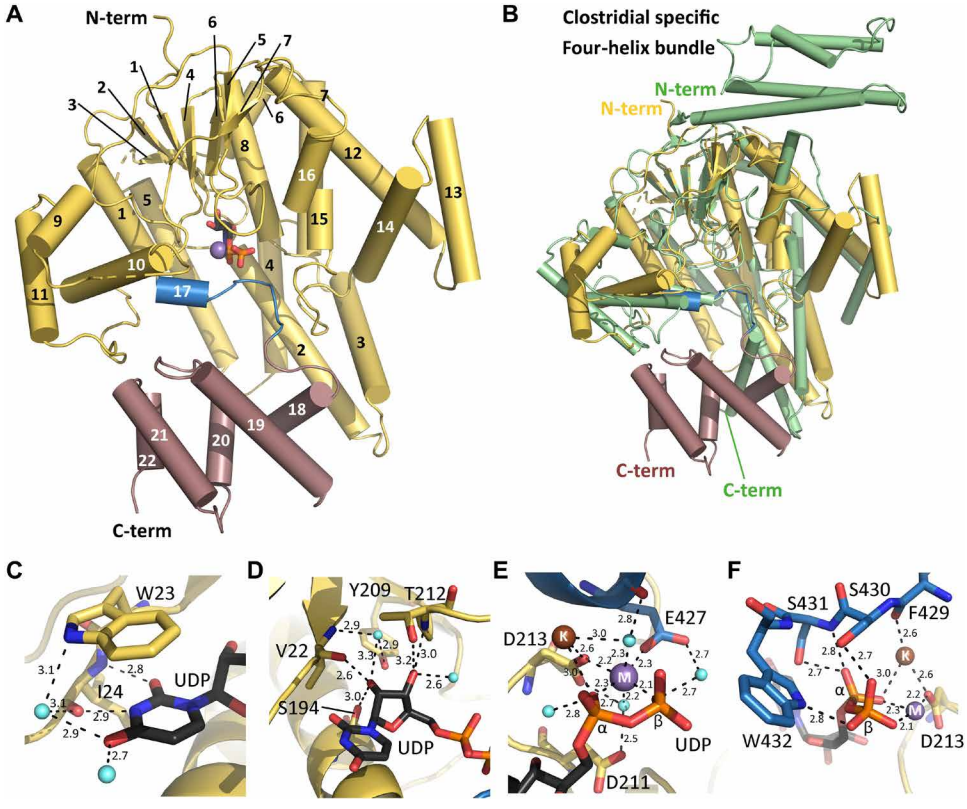

Fig. 3. Structure of YGT^G. (**A**) The YGT^G structure displays a typical GT-A glycosyltransferase fold (yellow) comprising a seven-stranded β sheet surrounded by α helices and a C-terminal five α-helical bundle (violet). UDP (black sticks) and Mn^{2+} (purple sphere) are bound centrally. Helix 17 and the loop that encloses the ligand binding site are highlighted in blue. (**B**) Structural superposition of YGT^G [colored as in (A)] with TcdB from *C. difficile* [Protein Data Bank (PDB) ID: 2BVL, green] showing the GT-A glycosyltransferase fold. While the N-terminal four-helix bundle of TcdB is absent in YGT^G, four helices at the C terminus of YGT^G are not conserved in clostridial toxins. (**C** to **F**) Closeup views of the active site showing the binding mode of UDP (black) with Mn^{2+} and K^+ ions represented as spheres (purple and brown, respectively) and YGT^G represented as a cartoon with relevant residues in sticks and colored as in (A). (C) The uridine base moiety is coordinated by a π-stacking interaction with Trp^{23} and by several direct and water-mediated hydrogen bonds (dashed lines). (D) The ribose moiety is coordinated by a series of hydrogen bonds with its hydroxyl groups. (E) The diphosphate from UDP is stabilized via interactions with the Mn^{2+} ion. Mn^{2+} is coordinated with aspartate side chains of the DXD motif, Glu^{427}, and water molecules. Note the presence of a K^+ ion in close vicinity. (F) The C-terminal loop of the GT-A fold encloses the nucleotide-binding pocket comprising direct interactions between the diphosphate moiety and Ser^{430}, Ser^{431}, and Trp^{432}.

Inhibition of GTP hydrolysis by YART-induced ADP-ribosylation

ADP-ribosylation of Rab proteins by YART occurs in a highly conserved glutamine residue that is essential for guanosine triphosphate (GTP) hydrolysis. To study the consequences of ADP-ribosylation on GTP hydrolysis, we used Rab5, although it was not the preferred substrate of YART, because GTPase-activating proteins (GAPs) are available for Rab5 but not for Rab31. Under basal conditions, ~40 to 50% of GTP bound to Rab5 was hydrolyzed after 30 min. Preincubation of Rab5 with YART^A in the presence of high concentrations of NAD^+ (400 μM) reduced basal GTP hydrolysis to ~20% (Fig. 5A). Inhibition of GTP hydrolysis was not observed when the inactive mutant YART^A E160A was used. The addition of the GAP (RabGAP5) largely increased hydrolysis of Rab5-bound GTP to >90% (remaining Rab5-bound GTP, ~5%) (Fig. 5A). This effect was strongly inhibited by YART^A-induced ADP-ribosylation (remaining GTP, ~65%). Again, the inactive mutant YART^A E160A was without effect. Thus, ADP-ribosylation blocks GTP hydrolysis and causes activation of Rab5 protein.

Effects of YART and YGT expression on Rab5 effector interaction

Next, we studied the effects of YART and YGT in intact cells. We coexpressed active or inactive YART^A with active or inactive YGT^G in HeLa cells together with Flag-tagged Rab5. To analyze the consequences of ADP-ribosylation and/or glycosylation of Rab5 on the interaction with its effectors, we performed pull-down assays of Flag-tagged Rab5 with the Rab5-binding domains (R5BDs) of the effectors EEA1 (early endosome antigen 1) and Rabenosyn-5. The amount of precipitated Rab5 was detected by an anti-Flag antibody. As shown in Fig. 5B, expression of active YART^A together with inactive YGT^G largely increased the interaction of R5BDs with Rab5 as compared with controls (e.g., expression of inactive YART^A and inactive YGT^G), indicating strong activation of Rab5. When both YART^A and YGT^G were expressed as active proteins, the R5BD pulldown of Rab5 was significantly reduced compared with active YART^A and inactive YGT^G. Last, expression of active YGT^G in the presence of inactive YART^A resulted in minor pulldown of Rab5. Thus, all these data are in agreement with an activation of Rab5 by YART^A and its inactivation by YGT^G.

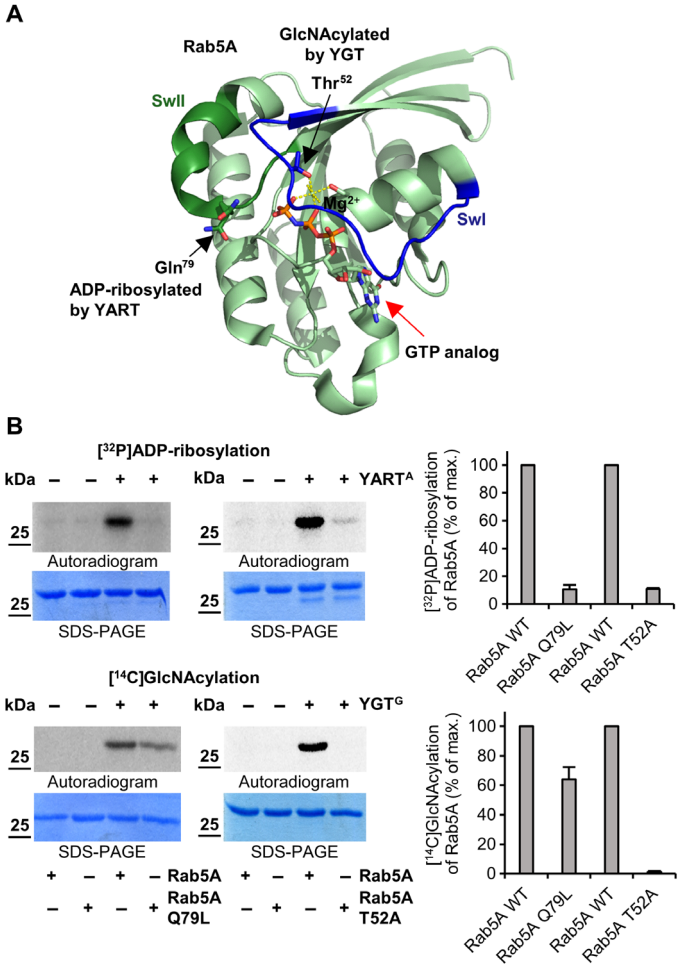

Fig. 4. YART- and YGT-induced modifications of Rab5. (**A**) Localization of the sites of Rab5A that are modified by YGT-induced GlcNAcylation and YART-induced ADP-ribosylation. Modification sites are from MS analyses and introduced into the Rab5A structure (PDB ID: 1N6H). Switch-1 (SwI) and switch-2 (SwII) regions are indicated in blue and dark green, respectively. Light green spheres represent the Mg^{2+} ion, while guanosine triphosphate (GTP) (or a GTP analog) is indicated by red arrow. While YGT modifies Rab5 in Thr^{52} (black arrow) by GlcNAcylation, YART ADP-ribosylates Gln^{79} (black arrow). (**B**) ADP-ribosylation or GlcNAcylation of mutant Rab5 proteins. Wild-type and mutant Q79L or T52A Rab5 proteins (each 2 μg) were incubated with 1 μM $YART^A$ or YGT^G, [^{32}P]NAD$^+$, or UDP-[^{14}C]GlcNAc for 1 hour at 21°C. The modifications of proteins were analyzed by SDS-PAGE and phosphorimaging. The amount of modified Rab proteins was normalized to wild-type Rab protein. Means (±SD) of three independent experiments and one representative autoradiogram and Coomassie gel are shown.

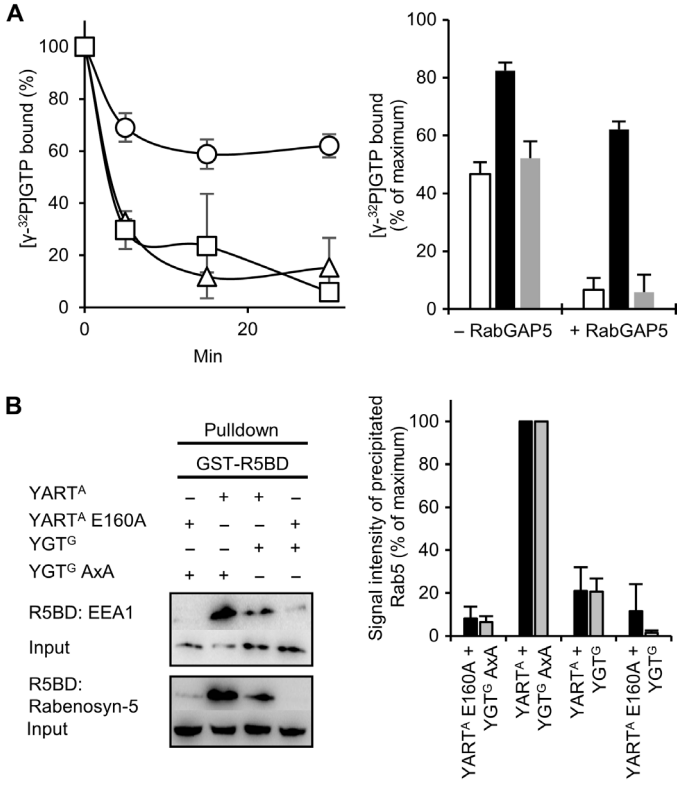

Fig. 5. Functional consequences of Rab5-induced modifications by YART and YGT. (**A**) YART effects on GTP hydrolysis by Rab5. Rab5A was ADP-ribosylated by active $YART^A$ or inactive $YART^A$ E160A and loaded with [γ-^{32}P]GTP. Left: RabGAP5-stimulated GTP hydrolysis (time course) by Rab5A pretreated with $YART^A$ (○), with $YART^A$ E160A (□) or untreated control (△). Right: GTP hydrolysis after 30 min with or without RabGAP5 (untreated control, white column; $YART^A$ pretreatment, black column; $YART^A$ E160A pretreatment, gray column). Data are means ± SD ($n = 3$). (**B**) Pulldown of Rab5A by the R5BDs of EEA1 and Rabenosyn-5. Rab5A (Flag-tagged) was coexpressed overnight in HeLa cell with active $YART^A$ and YGT^G or with the inactive mutants $YART^A$ E160A and YGT^G AXA. Cell lysates were incubated with GST-R5BD–coupled beads (30 min). Thereafter, beads were precipitated and washed, and interacting proteins were analyzed by SDS-PAGE and Western blot. Immunoblots with anti-Flag antibody before (input) and after pulldown are shown. Left: One representative experiment. Right: Results of three independent experiments with EEA1 (black column) or with Rabenosyn-5 (gray column) (data are means ± SD). The amount of precipitated Rab5 was normalized to the pulldown of Rab5 after coexpression with $YART^A$ and YGT^G AXA.

It has been reported that overexpression of Rab5 or expression of constitutively active Rab5 induces enlargement of early endosomes (*24*, *25*). Therefore, we studied the effects of YART and YGT on the size of vesicles associated with Rab5. To this end, mCherry-tagged Rab5A (mCherry-Rab5) was expressed in HeLa cells. In addition, the constructs contained a Flag tag for detection by Western blotting. When mCherry-Rab5A was coexpressed with the active ADP-ribosyltransferase domain of YART [green fluorescent protein (GFP)–$YART^A$], the immunofluorescence microscopic analysis revealed that the area of mCherry-Rab5–associated vesicles was significantly increased as compared with coexpression with the inactive YART mutant (GFP-$YART^A$ E160A) (Fig. 6, A and C). Next, we tested the influence of YGT on Rab5-associated vesicles in the presence of active and inactive YART (Fig. 6, B and D). When the active YART domain (GFP-$YART^A$) was expressed together with the inactive glycosyltransferase domain of YGT (GFP-YGT^G AXA), vesicle size was increased. However, when activated glycosyltransferase domain (GFP-YGT^G) was expressed, no labeled vesicles were detected, and mCherry-Rab5 was equally distributed in the cytosol. The same result was obtained after expression of active YGT^G together with inactive YART mutant (GFP-$YART^A$ E160A). Western blot analysis revealed efficient coexpression of the various constructs under the conditions used (Fig. 6E). Again, these findings supported the notion that YART activates Rab5, thereby increasing the fusion and enlargement of Rab5-associated vesicles, whereas YGT inactivates Rab5, which appears to dominantly block Rab5 interaction with vesicles.

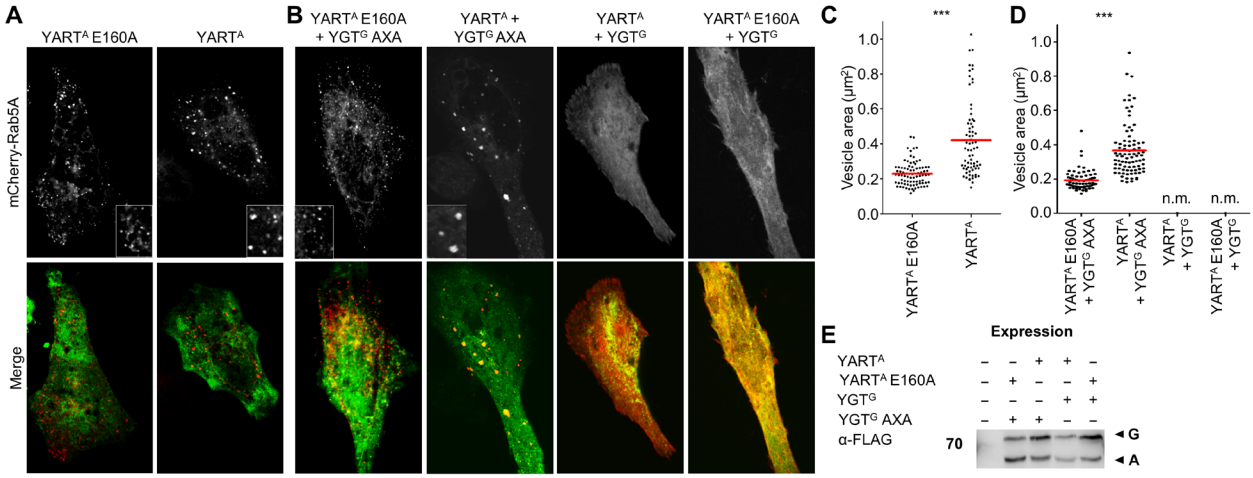

Fig. 6. Effect from YART and YGT on the Rab5A distribution in HeLa cells. HeLa cells were transiently transfected overnight with mCherry-C1-Rab5A (top; red) together with the indicated pEGFP-C1-toxin constructs (green). Afterward, cells were washed and incubated at 21°C for an additional 3 hours. Insets show in detail Rab5A-vesicle structure. Pictures are representative of three independent experiments. Scale bar, 10 µm. (**A**) Effects of YART^A or YART^A E160A on the distribution of overexpressed Rab5A. (**B**) Effects of active YART^A and YGT^G and inactive YART^A E160A and YGT^G AXA on the distribution of overexpressed mCherry-C1-Rab5A. (**C**) Quantification by MetaMorph imaging software of the size of mCherry-C1-Rab5A vesicles in the presence of the active (YART^A) or inactive ADP-ribosyltransferase domain (YART^A E160A). Cells of view are ≥20, and $n = 3$. Unpaired two-sample t test was used (***$P < 0.001$). (**D**) Quantification of (B) as described in (C). n.m., not measurable. (**E**) For analysis of the expression of pEGFP-C1-toxin constructs, HeLa cells were lysed after transfection and expression. Proteins were analyzed by SDS-PAGE, Western blotting, and immunostaining with anti-FLAG tag antibody. G indicates GFP-YGT^G and GFP-YGT^G AXA; A indicates GFP-YART^A and GFP-YART^A E160A.

DISCUSSION

Here, we detected in *Y. mollaretii* two *Yersinia* toxins called YGT and YART that were largely related to CGTs. While YGT was only found in *Y. mollaretii* (strain ATCC 43969), YART-like proteins (~95% sequence identity) were also detected in a *Yersinia massiliensis* and a *Yersinia intermedia* strain. Both proteins (YGT and YART) comprised the typical polymodular structure of CGTs with an N-terminal enzyme domain, followed by an autoprotease domain and a C-terminal translocation and binding domain (*1*). In contrast to most CGTs, YGT and YART have no C-terminal CROP domains. Thus, the putative *Yersinia* toxins resemble the structure of *C. perfringens* toxin TpeL, which also lacks CROPs (*7*). Similar to TcdB (*3*), both *Yersinia* proteins increased electric conductance in black lipid membranes at low pH, suggesting pore-forming activity involved in membrane translocation. Both YART and YGT share amino acid sequences (amino acids 1080 to 1093 of YGT and amino acids 905 to 918 of YART) with *C. difficile* toxins, which appear to be essential for pore formation of TcdB (*11*). Exchange of Leu^{917} and Leu^{1092} of YART and YGT, respectively, which are equivalent to Leu^{1106} in TcdB, blocked membrane activity. Thus, YART and YGT are probably translocated across membranes by the same molecular mechanism as CGTs. Further studies are necessary to reveal the typical low pH–dependent uptake of the toxins from endosomes and to exclude delivery mechanisms directly involving bacterial secretion systems.

Similar to CGTs (*4*, *5*), YGT and YART have autocleavage activity in the presence of $InsP_6$. While YART cleaves behind the ADP-ribosyltransferase domain, YGT cuts downstream of the autoprotease domain after Leu^{781}. Change of this residue to alanine blocked cleavage. These findings suggest that the glycosyltransferase is released into the cytosol together with the autoprotease domain. Whether this is of functional importance remains to be studied.

The N-terminal enzyme domain of YART (YART^A) has ADP-ribosyltransferase activity. This finding shows that the toxin activity of CGT-like toxins is not coupled to only one type of enzyme activity (e.g., glycosyltransferase activity). We found that YART specifically modifies Rab proteins. Rab31 was the highly preferred substrate followed by Rab17 and Rab5. Notably, Ras and Rho proteins were not ADP-ribosylated by YART. The identification of Rab31 protein as target of a bacterial toxin is unique. So far, only *Pseudomonas aeruginosa* exoenzyme S (ExoS), which is a type III secretion effector, has been reported to ADP-ribosylate Rab5 (*26*). However, ExoS ADP-ribosylates multiple target proteins, including various low–molecular mass GTPases (Rho, Ras, and Rab), ERM (ezrin-radixin-moesin) proteins, and vimentin (*26*). Moreover, modification of Rab proteins by ExoS occurs at multiple sites. By contrast, ADP-ribosylation of Rab31 and Rab5 by YART is restricted to Gln^{64} and Gln^{79}, respectively, which are functionally equivalent glutamine residues. This glutamine residue is conserved in nearly all small GTPases and involved in GTP hydrolysis. The function of the glutamine residue is the optimal positioning of the nucleophilic water molecule for attacking the γ phosphate of GTP and to stabilize the transition state of GTP hydrolysis (*27*). Therefore, ADP-ribosylation inhibits hydrolysis of GTP even after stimulation of the GTPase activity by RabGAP5.

Similar to CGTs, the YGT^G has glycosyltransferase activity by using UDP-GlcNAc as sugar donor. Both glucosylation and GlcNAcylation are observed within the family of CGTs (*13*). While *C. difficile* toxins (TcdA and TcdB) use UDP-glucose, *C. novyi* α-toxin and *C. perfringens* TpeL prefer UDP-GlcNAc like YGT (*13*). Similarly, as found for YART, YGT targets Rab5 and Rab31, which were modified in Thr^{52} and Thr^{36}, respectively. These functionally equivalent residues are located in the switch I region of the GTPases and have a crucial role in Mg^{2+} ion coordination and nucleotide binding. Modification of Rab at this site is unique for YGT. Notably, CGTs (e.g., TcdA and TcdB) modify the equivalent residue (Thr^{37} or Thr^{35}) in Rho proteins (*6*). Other CGTs modify

Ras proteins like *C. sordellii* lethal toxin (TcsL) and *C. perfringens* toxin TpeL (*7*, *13*).

In line with the functional similarity of YGT^G with CGTs, the YGT^G structure has a typical GT-A glycosyltransferase fold and shows highest structural similarity to clostridial toxins (*14*–*16*) including lethal toxin, TcdA and TcdB, and α-toxin. In contrast to these, YGT^G includes a C-terminal five-helix bundle of yet unknown function. The canonical core GT-A glycosyltransferase, which harbors the Rossmann fold–like and its nucleotide-binding site, is also structurally similar to the smaller glycosyltransferase domain of PaTox (*18*) from *P. asymbiotica* as well as to the arginine glycosylating effector proteins SseK1, SseK3, and NleB (*19*, *20*). The structure of UDP-bound YGT^G sheds light on the nucleotide-binding mode reflecting the situation after the glycosyltransferase reaction has occurred. The binding mode ensures nucleoside specificity. The conserved DXD motif and a divalent cation, here referred to as a manganese ion, position the diphosphate moiety. Overall, the binding mode is similar to those reported for clostridial toxins (*14*).

The structures of ligand-free and ligand-bound YGT^G reveal two conformations of the terminal loop, which covers the diphosphate moiety when the nucleotide is bound and leaves the binding pocket open in ligand-free state. The closed conformation is similar to those in glycosyltransferase structures from TcdA (*15*) and lethal toxin (*16*) in the presence of UDP-glucose. Consistent with the ligand-free YGT^G structure, in nucleotide-free structures of α-toxin from *C. novyi* and of TcdA from *C. difficile* (*15*, *16*, *23*), the loop is displaced, and the binding site is open. Together, clostridial and YGT^G structures show a consistent conformational change of the so-called lid loop from open conformation in the nucleotide-free state to closed conformation when the nucleotide is present.

A notable feature of the UDP-bound YGT^G structure is the presence of a potassium ion at the ligand-binding site. Potassium strongly enhances the activity of CGTs (*21*–*23*) and YGT. Yet so far, the relevant ion-binding site was not structurally resolved. Because the potassium ion in YGT^G is directly coordinated by the DXD motif's Asp^{213} side chain, which also coordinates the manganese ion, the potassium ion is likely to affect the charge equilibration in the binding site. The ion also interacts with residues of the lid loop in the closed state and may help to stabilize ligand binding. We suggest that the identified potassium ion–binding site is the basis for enhanced glycosyltransferase activity in clostridial and related toxins.

Rab proteins are master regulators of endosome fusions (*28*). Canonically, the presence of Rab5 and its effectors like EEA1 defines prototypic early endosomes (*29*). The GTPase controls the maturation of phagosomes to phagolysosomes, which have major antimicrobial activity (*30*). Accordingly, various studies report on a role of Rab5 in host-pathogen interactions, including pathogens such as *Listeria monocytogenes* (*31*), *P. aeruginosa* (*32*), *Salmonella* (*33*), and *Yersinia* (*34*). Rab31 (also called Rab22B) belongs to the Rab5 subfamily. It mainly localizes to the trans-Golgi network and is probably involved in the anterograde exit from the trans-Golgi network to the cell membrane (*35*). Considering that many *Yersinia* species (e.g., *Y. pestis*, *Y. pseudotuberculosis*, *Y. enterocolitica*, and *Y. ruckeri*) are facultative intracellular pathogens (*36*, *37*), the same is probably true for *Y. mollaretii*. Our coexpression studies show that YART and YGT regulate Rab proteins in a bidirectional (inverse) manner. Expression of $YART^A$ largely increased the level of activated Rab5. Similarly, expression of YART increased the size of Rab5-associated vesicles, which is a consequence of constitutive activation of Rab5 (*24*, *25*). These effects were inhibited by YGT. Moreover, YGT caused equal distribution of labeled Rab5 in the cytosol without any vesicle association, indicating inactivation of Rab5. Rab5 and Rab31 are likely involved in invasion and intracellular infection of *Yersinia*. Thus, we speculate that YART- and YGT-induced activation and/or inhibition of Rab proteins occur in a time- and space-dependent manner to optimize the survival of the pathogen.

Y. mollaretii have been isolated from human feces, fresh water, animal feces, and intestines and foods (*38*). The bacteria are also found in the oral microbiome of children (*39*). So far, however, a pathogenic role of *Y. mollaretii* for humans is not known. Specific *Yersinia* (e.g., *Yersinia entomophaga*) are pathogenic for insects (*40*). This is also true for *Y. mollaretii* (*41*). It remains to be studied whether YART and YGT are virulence factors, which are important for host-pathogen interaction in insects.

MATERIALS AND METHODS

Cell culture, preparation of mammalian cell lysates, and immunostaining

HeLa cells were grown in Dulbecco's modified Eagle's medium in a humidified atmosphere of 5% CO_2 at 37°C. The media contained 10% fetal calf serum, penicillin (4 mM), and streptomycin (4 mM). For preparation of cell lysate, cells were washed with ice-cold phosphate-buffered saline (PBS) and lysed in the indicated buffer for 5 min on ice. Afterward, the cell lysate was transferred into a 1.5-ml tube and cleared by centrifugation (10 min, 4°C, 20,000*g*). The supernatants were used for the following experiments. After separation of proteins by SDS–polyacrylamide gel electrophoresis (PAGE) and Western blotting, the proteins were detected by specific antibodies. Horseradish peroxidase–conjugated donkey anti-mouse immunoglobulin G (H&L) (610-703-124; Rockland) or goat anti-rabbit immunoglobulin G (H&L) (no. 7074, Cell Signaling) antibody was used as a secondary antibody. Antibody signals were detected by enhanced chemiluminescence using the LAS-4000 reader (Fujifilm) and quantified with MultiGauge software (FujiFilm).

Yeast culture conditions

Yeast strains were cultivated on minimal YNB medium (0.67% yeast nitrogen base without amino acids; Difco) containing 2% glucose or galactose and adapted from the specific *S. cerevisiae* strain requirements, with the suitable supplements (uracil, tryptophan, adenine, or leucine) completed. For successful yeast transformation, the lithium acetate method (*42*) was used.

Preparation of yeast lysates and membrane fractions

Yeast cells were cultivated in YPD (yeast extract–peptone–dextrose) medium or in selective SD (supplemental dextrose) medium on a shaker at 30°C; afterward, the cells were harvested by centrifugation at 4000 rpm for 10 min at 4°C. The pellet was washed once with ice-cold water. Then, the pellet was resuspended in a minimal volume of lysis buffer [50 mM tris-HCl (pH 7.4), 150 mM NaCl, and Protease Inhibitor Cocktail (Roche Diagnostics GmbH, Mannheim, Germany)], and the cells were disrupted using acid-washed glass beads (425 to 600 μm, Sigma-Aldrich) by vortexing of the 1:1 cell pellet–beads mixture for 1 min at maximal power. After 1 min on ice, the procedure was repeated six times. Last, the whole mixture was centrifuged at 20,000*g* for 15 min at 4°C, and the protein content of the supernatant was determined by using the bicinchoninic acid Protein Assay

Kit (Life Technologies, Waltham) according to the manufacturer's protocol. For separating the membrane fraction, the supernatant was additionally ultracentrifuged for 1 hour at 100,000*g* at 4°C, and the membrane pellet was resuspended in buffer [25 mM tris-HCl (pH 7.5) and 1 mM EDTA].

Cloning, expression, and purification of proteins

Cloning and recombinant protein production were performed in *Escherichia coli* TG1 and BL21, respectively. *S. cerevisiae* MH272-3fα (ura3, leu2, his3, trp1, and ade2) and pESC-Ura galactose-inducible expression vectors were obtained from Stratagene (Agilent, Frankfurt, Germany). The various mutants were constructed by site-directed mutagenesis using QuikChange kit (Stratagene) according to the manufacturer's instructions, with the exception that the Velocity DNA Polymerase (Bioline) was used. The constructs were checked by DNA sequencing (Eurofins GATC Biotech GmbH, Konstanz, Germany). Primers (Biomers, Ulm; Apara Bioscience, Denzlingen) and gBlock Gene fragments (Integrated DNA Technologies, USA) used for cloning are listed in table S3. For purification, the *E. coli* strain BL21 was transformed with the corresponding plasmids and was grown at 37°C in Luria-Bertani broth supplemented with the respective antibiotics [ampicillin (100 μg/ml) or kanamycin (30 μg/ml)] until an optical density of A_{600} = 0.5 to 0.8. The expression of the proteins was induced by adding isopropyl-β-D-thiogalactopyranoside (IPTG) (Roth, Karlsruhe), and bacteria were grown for indicated times at the given temperatures (table S4). The cells were harvested by centrifugation with 6000 rpm for 15 min and resuspended in the indicated lysis buffer with DNAse (deoxyribonuclease; 5 μg/ml), lysozyme (1 mg/ml), and 1 mM phenylmethylsulfonyl fluoride (PMSF) (Sigma-Aldrich). The bacterial cells were lysed by using an ultrasonic homogenizer and centrifuged for 45 min (14,000 rpm, 4°C). The proteins were purified from the supernatant by nickel affinity purification or Glutathione Sepharose 4B (GE Healthcare) according to the tag of the protein (table S4). Proteins were stored in the indicated buffers at −80°C (table S4).

Black lipid bilayer experiments

Membrane insertion and pore activity were measured using black lipid membranes composed of diphytanoyl phosphatidylcholine (DiPhPC). Black lipid bilayer experiments were performed as described previously (*3*). The instrumentation consisted of a Teflon chamber divided into two compartments by a thin wall and connected by a small circular hole (~0.4 mm^2). The aqueous solutions of both chambers contained 1 M KCl and were buffered with 20 mM tris-HCl (pH 7.4). After painting a 1% solution of DiPhPC (Avanti Polar Lipids, Alabaster, AL) dissolved in *n*-decane across the hole to form a membrane, the toxins (3.5 nM) were added to one side of the membrane (the cis side). After 5 min, by the addition of 1.85% HCl into the same compartment containing the toxins, the pH drop to pH 4.8 was obtained. The current of the membrane was measured by using Ag/AgCl electrodes (with salt bridges) switched in series with a voltage source and a homemade current amplifier. The applied membrane potential was −50 mV at room temperature. The signal was recorded on a strip chart recorder (Rikadenki, Freiburg, Germany).

In vitro autocleavage assay

For the in vitro autocleavage assay, 2 μg of full-length toxins or toxin fragments was incubated in cleavage buffer [100 mM tris-HCl (pH 7.4)] with the indicated concentrations of $InsP_6$. After incubation for 1 hour at 37°C, the reaction was stopped by adding Laemmli buffer and boiling for 5 min at 95°C. The visualization of the cleavage products was done by SDS-PAGE, subsequent Western blotting, and anti-His (no. 2365S, Cell Signaling) antibody staining.

Spot test assay

For testing the toxicity of YART and YGT in *S. cerevisiae*, yeast growth on agar plates was analyzed. Therefore, fivefold serial dilutions of yeast cultures were spotted onto YNB agar supplemented with glucose or galactose and with adenine, tryptophan, leucine, and uracil. Yeast was incubated for 3 days at 30°C.

Hydrolysis of UDP-glucose and UDP-GlcNAc by YGT

For determination of UDP-glucose hydrolysis, YGT^G was incubated with UDP-[^{14}C]Glc or UDP-[^{14}C]GlcNAc (at indicated concentrations) in the reaction buffer, containing 50 mM Hepes (pH 7.5), 100 mM KCl, 2 mM $MgCl_2$, and 1 mM $MnCl_2$. One-microliter samples were taken at the indicated time points and subjected to PEI (polyethyleneimine)–cellulose thin-layer chromatography (Merck, Darmstadt, Germany). To separate hydrolyzed [^{14}C]glucose from UDP-[^{14}C]glucose, 0.2 mM LiCl was used as mobile phase, and the samples were allowed to run for 8 min. Eventually, the plates were dried and analyzed with the phosphorimager (Typhoon FLA 7000, GE Healthcare, Freiburg, Germany), and radioactive samples were quantified by using MultiGauge software.

Glycosylation assay

For the glycosylation assay, cell lysate or recombinant GTPases were incubated with recombinant YGT^G or its mutants and 10 μM UDP-[^{14}C]GlcNac in a buffer containing 50 mM Hepes (pH 7.5), 100 mM KCl, 2 mM $MgCl_2$, 1 mM $MnCl_2$, and BSA (0.1 mg/ml) at 21°C for the indicated time. Analyses of modified proteins were done by SDS-PAGE and afterward by phosphorimaging (Typhoon FLA 7000, GE Healthcare, Freiburg, Germany).

ADP-ribosylation reaction

Cell lysate or recombinant GTPases were incubated for the indicated time at 21°C with 1 μM [^{32}P]NAD^+ and $YART^A$ in ADP-ribosylation buffer [20 mM tris-HCl (pH 7.4), 1 mM EDTA, and 5 mM $MgCl_2$]. All radiolabeled proteins were detected by SDS-PAGE and subsequent phosphorimaging (Typhoon FLA 7000, GE Healthcare, Freiburg, Germany).

GTP hydrolysis assay

First, Rab5A (10 μM) was ADP-ribosylated by active $YART^A$ or inactive $YART^A$ E160A (each 1 μM) in the presence of 400 μM NAD^+ in a buffer containing 50 mM Hepes (pH 7.5), 100 mM KCl, 2 mM $MgCl_2$, 1 mM $MnCl_2$, and BSA (0.1 mg/ml) for 60 min at 24°C. Afterward, for loading of Rab proteins, 5 μl of 10-fold buffer A [500 mM Hepes (pH 7.4), BSA (10 mg/ml), 10 mM dithiothreitol (DTT), and 10 mM adenosine triphosphate], 1 μl of 50 mM EDTA, 1 μl of 25 mM $MgCl_2$, 25 μl of 10 μM [γ-^{32}P]GTP [in 50 mM tris-HCl (pH 8.0), 1 mM DTT, 1 mM ATP, and 10 μM GTP], 13 μl of H_2O, and 5 μl of 10 μM pretreated Rab5A were mixed on ice and then incubated for 45 min at 24°C. Then, 10 μl of the preloaded Rab was added to a 90-μl reaction mix (buffer A plus 5 mM $MgCl_2$, and 1 mM GTP). GAP reaction was started by the addition of 1 pmol of the MBP (maltose-binding protein)–tagged RabGAP5. GTP hydrolysis was

performed at 16°C. At indicated times, 10-µl samples were removed and added to 950-µl ice-cold stopping buffer [20 mM tris-HCl (pH 8.0), 100 mM NaCl, and 5 mM $MgCl_2$]. Bound radioactively labeled GTP was measured using a nitrocellulose filter-binding assay (*10*).

Effector pull-down assay

The effector pull-down was performed as described previously (*43*) with the exception that the HeLa cells were transfected with human Flag-Rab5A [a gift from Q. Zhong (plasmid no. 28043, Addgene; http://n2t.net/addgene:28043; RRID: Addgene_28043)] and in addition with the different toxin constructs. The transfection was done according to the manufacturer's instructions with Lipofectamine 2000 (Thermo Fisher Scientific, Karlsruhe, Germany). Data were obtained by SDS-PAGE, subsequent Western blotting, and anti-Flag (no. 14793S, Cell Signaling) antibody staining.

Expression of Rab5A, YART, and YGT in HeLa cells

HeLa cells were seeded at a density of 3.5×10^5 cells per well in six-well tissue culture plates. After settling down, cells were transfected with the mCherry-C1-Rab5A construct together with indicated pEGFP-C1-toxin constructs. The transfection was done by using Lipofectamine 2000 (Thermo Fisher Scientific, Karlsruhe, Germany) according to the manufacturer's protocol. After overnight culture, HeLa cells were washed with PBS and Dulbecco's modified Eagle's medium containing the described additives. Afterward, HeLa cells were incubated in a humidified atmosphere of 5% CO_2 at 21°C for 3 hours. Then, the cells were washed with PBS, fixed for 15 min with 4% paraformaldehyde in PBS, and washed again with PBS (all was done at room temperature). Last, cells were dried and embedded with Mowiol (Merck, Darmstadt, Germany) for microscopy.

Microscopy and imaging acquisition

Confocal fluorescence microscopy was performed with an Axiovert 200M microscope (Carl Zeiss, Jena, Germany), driven by the VisiView (Visitron, Puchheim, Germany) imaging software with plan-apochromat objectives, a Yokogawa CSU-X1 spinning disk confocal head with emission filter wheel, and a CoolSNAP HQ2 digital camera with 488- and 561-nm laser lines. Images were processed with MetaMorph imaging software (Universal Imaging, NY).

YGT crystallization and x-ray diffraction data collection

Before crystallization, YGT^G [final product after TEV (tobacco etch virus)–cleavage Gly-$YGT^{G\ 2–520}$] was concentrated to 15 mg/ml as estimated by Bradford assay. Vapor diffusion crystallization assays were performed at 4°C and at 20°C mixing 150 µl of YGT or YGT supplemented with 2 mM UDP and 2 mM $MnCl_2$ and an identical volume of precipitant solution. Within a few days, needle-shaped crystals appeared in several conditions at 20°C. At 4°C, the crystallization process took up to a month, but the nucleation was lower, and thus larger crystals could be obtained. Large crystals of YGT supplemented with 2 mM UDP and 2 mM $MnCl_2$ were grown in 100 mM tris-HCl (pH 8.5), 200 mM sodium acetate, and 15% polyethylene glycol (PEG) 4000. Ligand-free YGT crystals grew as very thin needles in a condition containing 200 mM sodium formate and 20% PEG 3350. Crystals were cryoprotected by the stepwise addition of ethylene glycol–supplemented reservoir solution to a final concentration of about 15% of ethylene glycol before transfer in liquid nitrogen. All data collections were carried out at 100 K. Initial diffraction data were collected at beamline ID23-1 (ESRF, Grenoble, France). A dataset at 1.9-Å resolution was collected from a crystal of UDP and $MnCl_2$-supplemented YGT^G at beamline ID30A-3 (MASSIF3, ESRF) at an energy of 12.8 keV. A native SAD dataset at 6-keV energy was collected at beamline ID29 (ESRF) (table S1). Data from YGT crystals were collected at 12.4 keV on beamline PXI (SLS, Villigen, Switzerland) (table S1).

Data processing and structure determination using native SAD

X-ray diffraction data were processed with XDS and scaled with XSCALE (*44*). Phenix.AutoSol (*45*) was used to solve the phase problem using the native SAD method, and the data were collected at 6 keV. A total of 17 sites were identified corresponding after structure refinement to 13 sulfur atoms, 2 phosphor atoms, 1 manganese atom, and 1 potassium atom. About 400 residues were built automatically, and the structure was finalized by manual modeling in Coot (*46*) and refinement cycles using Phenix (*45*). The 1.9-Å resolution structure of YGT^G with bound UDP and Mn^{2+} was refined to final R_{work} and R_{free} values of 18.6 and 22.3%, respectively. About 97.4 and 2.6% of the residues are in the favored and in the allowed areas of the Ramachandran plot, respectively. No Ramachandran outlier is present in the structure. The latter includes one YGT^G molecule (resolved residues 12 to 150, 153 to 230, and 233 to 518) with 1 UDP molecule, 1 manganese ion, 1 potassium ion, 8 ethylene glycol molecules, and 408 water molecules. This high-resolution structure was used as a molecular replacement search model to solve the phase problem of the ligand-free YGT^G structure using the program Phaser (*47*). The crystal belongs to another space group and has two monomers in the asymmetric unit. Several cycles of manual modeling and refinement using the program Buster (*48*) were required to obtain the final structure. Noncrystallographic symmetry was used in initial refinement steps, and the 1.9-Å resolution structure was used as reference model. The final structure shows R_{work} and R_{free} of 22.7 and 24.9%, respectively, with 95.8 and 3.9% of the residues in the most favored and allowed regions of the Ramachandran plot. Only four residues are in the disallowed regions of the Ramachandran plot. In the structure, one monomer comprises residues 12 to 430 and 435 to 519, while the second monomer has a few disordered short peptides and comprises residues 12 to 150, 153 to 301, 304 to 340, 344 to 364, 366 to 473, and 475 to 516. Final coordinates were deposited in the Protein Data Bank with accession codes 6RTG and 6RTH for the UDP-bound and ligand-free YGT^G, respectively. The DALI server (*49*) was used to analyze structural homology. The PyMOL Molecular Graphics System, version 2.3.0, Schrödinger LLC was used to prepare the figures.

NanoLC-MS/MS analysis

Ten micrograms of Rab5A or 8 µg of Rab31 was incubated for 4 hours at 21°C, followed by overnight incubation at 4°C with 400 µM NAD^+ and 8.5 µM $YART^A$. Afterward, the sample was reduced with 50 mM DTT and alkylated with 120 mM iodoacetamide before SDS-PAGE. For YGT, 10 µg of Rab5A was incubated for 4 hours at 21°C. Then, the reaction mix was incubated overnight at 4°C with 10 µM UDP-GlcNAc and 500 nM YGT^G. For cleavage analysis, $YART^{1–632}$ and $YGT^{1–1998}$ (each 4 µg of protein) were incubated for 1 hour at 37°C with 10 mM $InsP_6$, followed by SDS-PAGE.

The excised gel bands were destained with 30% acetonitrile in 0.1 M NH_4HCO_3 (pH 8), shrunk with 100% acetonitrile, and dried in a vacuum concentrator (Concentrator 5301, Eppendorf, Germany).

Digests were performed with 0.1 µg of trypsin respectively elastase per gel band overnight at 37°C in 0.1 M NH_4HCO_3 (pH 8). After removing the supernatant, peptides were extracted from the gel slices with 5% formic acid, and extracted peptides were pooled with the supernatant.

Nano liquid chromatograyphy–tandem MS (NanoLC-MS/MS) analyses were performed on an Orbitrap Fusion (Thermo Fisher Scientific) equipped with an EASY-Spray Ion Source and coupled to an EASY-nLC 1000 (Thermo Fisher Scientific). Peptides were loaded on a trapping column (2 cm by 75 µm ID, PepMap C18, 3-µm particles, 100-Å pore size) and separated on an EASY-Spray column (50 cm by 75 µm ID, PepMap C18, 2-µm particles, 100-Å pore size) with a 30-min linear gradient from 3 to 40% acetonitrile and 0.1% formic acid.

Both MS and MS/MS scans were acquired in the Orbitrap analyzer with a resolution of 60,000 for MS scans and 15,000 for MS/MS scans. A mixed ETD (electron transfer dissociation)/HCD (high-energy collision dissociation) method was used. HCD fragmentation was applied with 35% normalized collision energy. For ETD, calibrated charge-dependent ETD parameter was applied. A top-speed data-dependent MS/MS method with a fixed cycle time of 3 s was used. Dynamic exclusion was applied with a repeat count of 1 and an exclusion duration of 10 s; singly charged precursors were excluded from selection. Minimum signal threshold for precursor selection was set to 50,000. Predictive AGC (automatic gain control) was used with a target value of 2×10^5 for MS scans and 5×10^4 for MS/MS scans. EASYIC was used for internal calibration.

Mascot Distiller 2.5 was used for raw data processing and generating peak lists, essentially with standard settings for the Orbitrap (high/high settings). Mascot Server 2.5 was used for database searching with the following parameters: peptide mass tolerance, 10 parts per million; MS/MS mass tolerance, 0.02 Da; enzyme, "trypsin" with three missed cleavage sites allowed for trypsin or "none" for elastase; fixed modification, carbamidomethyl (C); variable modifications, Gln->pyroGlu (N-terminal Q), oxidation (M), HexNAc (ST), and ADP-ribosylation (NQ). Database searching was performed against a custom database containing the protein sequences of interest.

Statistics

Results are presented as means ± SD of at least three independent experiments (unless otherwise stated). Student's *t* test was applied when two groups with normal distribution had to be compared. Statistical analyses were performed using GraphPad Prism version 5.04. $P < 0.05$ was considered statistically significant and marked with an asterisk ($^*P < 0.05$; $^{**}P < 0.01$; $^{***}P < 0.001$).

SUPPLEMENTARY MATERIALS

Supplementary material for this article is available at http://advances.sciencemag.org/cgi/content/full/6/11/eaaz2094/DC1

Fig. S1. Model of the domain architecture of YART and YGT, in comparison to *C. difficile* TcdB and *C. perfringens* TpeL.

Fig. S2. Processing, expression, and enzyme activity of YART and YGT.

Fig. S3. Topological representation of YGT^G and potassium ion coordination in the ligand-bound YGT^G structure.

Fig. S4. C-terminal loop of the glycosyltransferase domain encloses the nucleotide-binding site in the UDP-bound state and leaves it open in the ligand-free state.

Fig. S5. ETD MS/MS spectra.

Fig. S6. YART- and YGT-induced modifications of Rab31.

Table S1. Data collection and refinement statistics.

Table S2. Proteins structurally homologous to YGT^G as identified by DALI and showing a *Z* score higher than 10.

Table S3. Genomic DNA, primer, gblocks, plasmids, and vectors.

Table S4. Buffer and conditions of protein purification.

View/request a protocol for this paper from *Bio-protocol*.

REFERENCES AND NOTES

1. K. Aktories, C. Schwan, T. Jank, *Clostridium difficile* toxin biology. *Annu. Rev. Microbiol.* **71**, 281–307 (2017).
2. D. E. Voth, J. D. Ballard, *Clostridium difficile* toxins: Mechanism of action and role in disease. *Clin. Microbiol. Rev.* **18**, 247–263 (2005).
3. H. Barth, G. Pfeifer, F. Hofmann, E. Maier, R. Benz, K. Aktories, Low pH-induced formation of ion channels by *Clostridium difficile* toxin B in target cells. *J. Biol. Chem.* **276**, 10670–10676 (2001).
4. M. Egerer, T. Giesemann, T. Jank, K. J. Satchell, K. Aktories, Auto-catalytic cleavage of *Clostridium difficile* toxins A and B depends on cysteine protease activity. *J. Biol. Chem.* **282**, 25314–25321 (2007).
5. J. Reineke, S. Tenzer, M. Rupnik, A. Koschinski, O. Hasselmayer, A. Schrattenholz, H. Schild, C. von Eichel-Streiber, Autocatalytic cleavage of *Clostridium difficile* toxin B. *Nature* **446**, 415–419 (2007).
6. I. Just, J. Selzer, M. Wilm, C. von Eichel-Streiber, M. Mann, K. Aktories, Glucosylation of Rho proteins by *Clostridium difficile* toxin B. *Nature* **375**, 500–503 (1995).
7. M. Nagahama, A. Ohkubo, M. Oda, K. Kobayashi, K. Amimoto, K. Miyamoto, J. Sakurai, *Clostridium perfringens* TpeL glycosylates the Rac and Ras subfamily proteins. *Infect. Immun.* **79**, 905–910 (2010).
8. S. Atkinson, P. Williams, Yersinia virulence factors - a sophisticated arsenal for combating host defences. *F1000Res* **5**, 10.12688/f1000research.8466.1 (2016).
9. R. R. Rucker, Redmouth disease of rainbow trout (*Salmo gairdneri*). *Bull. Off Int. Epizoot* **65**, 825–830 (1966).
10. T. Jank, S. Eckerle, M. Steinemann, C. Trillhaase, M. Schimpl, S. Wiese, D. M. F. van Aalten, W. Driever, K. Aktories, Tyrosine glycosylation of Rho by *Yersinia* toxin impairs blastomere cell behaviour in zebrafish embryos. *Nat. Commun.* **6**, 7807 (2015).
11. Z. Zhang, M. Park, J. Tam, A. Auger, G. L. Beilhartz, D. B. Lacy, R. A. Melnyk, Translocation domain mutations affecting cellular toxicity identify the *Clostridium difficile* toxin B pore. *Proc. Natl. Acad. Sci. U.S.A.* **111**, 3721–3726 (2014).
12. B. Lüscher, M. Bütepage, L. Eckei, S. Krieg, P. Verheugd, B. H. Shilton, ADP-Ribosylation, a multifaceted posttranslational modification involved in the control of cell physiology in health and disease. *Chem. Rev.* **118**, 1092–1136 (2018).
13. T. Jank, Y. Belyi, K. Aktories, Bacterial glycosyltransferase toxins. *Cell. Microbiol.* **17**, 1752–1765 (2015).
14. D. J. Reinert, T. Jank, K. Aktories, G. E. Schulz, Structural basis for the function of *Clostridium difficile* toxin B. *J. Mol. Biol.* **351**, 973–981 (2005).
15. R. N. Pruitt, N. M. Chumbler, S. A. Rutherford, M. A. Farrow, D. B. Friedman, B. Spiller, D. B. Lacy, Structural determinants of *Clostridium difficile* toxin A glucosyltransferase activity. *J. Biol. Chem.* **287**, 8013–8020 (2012).
16. M. O. Ziegler, T. Jank, K. Aktories, G. E. Schulz, Conformational changes and reaction of clostridial glycosylating toxins. *J. Mol. Biol.* **377**, 1346–1356 (2008).
17. N. M. Chumbler, S. A. Rutherford, Z. Zhang, M. A. Farrow, J. P. Lisher, E. Farquhar, D. P. Giedroc, B. W. Spiller, R. A. Melnyk, D. B. Lacy, Crystal structure of *Clostridium difficile* toxin A. *Nat. Microbiol.* **1**, 15002 (2016).
18. T. Jank, X. Bogdanović, C. Wirth, E. Haaf, M. Spoerner, K. E. Böhmer, M. Steinemann, J. H. C. Orth, H. R. Kalbitzer, B. Warscheid, C. Hunte, K. Aktories, A bacterial toxin catalyzing tyrosine glycosylation of Rho and deamidation of Gq and Gi proteins. *Nat. Struct. Mol. Biol.* **20**, 1273–1280 (2013).
19. J. B. Park, Y. H. Kim, Y. Yoo, J. Kim, S.-H. Jun, J. W. Cho, S. El Qaidi, S. Walpole, S. Monaco, A. A. García-García, M. Wu, M. P. Hays, R. Hurtado-Guerrero, J. Angulo, P. R. Hardwidge, J.-S. Shin, H.-S. Cho, Structural basis for arginine glycosylation of host substrates by bacterial effector proteins. *Nat. Commun.* **9**, 4283 (2018).
20. D. Esposito, R. A. Günster, L. Martino, K. E. Omari, A. Wagner, T. L. M. Thurston, K. Rittinger, Structural basis for the glycosyltransferase activity of the *Salmonella* effector SseK3. *J. Biol. Chem.* **293**, 5064–5078 (2018).
21. W. P. Ciesla Jr., D. A. Bobak, *Clostridium difficile* toxins A and B are cation-dependent UDP-glucose hydrolases with differing catalytic activities. *J. Biol. Chem.* **273**, 16021–16026 (1998).
22. H. Genth, I. Schelle, I. Just, Metal ion activation of *Clostridium sordellii* lethal toxin and *Clostridium difficile* toxin B. *Toxins* **8**, 109 (2016).
23. N. D'Urzo, E. Malito, M. Biancucci, M. J. Bottomley, D. Maione, M. Scarselli, M. Martinelli, The structure of *Clostridium difficile* toxin A glucosyltransferase domain bound to Mn^{2+} and UDP provides insights into glucosyltransferase activity and product release. *FEBS J.* **279**, 3085–3097 (2012).
24. C. Bucci, R. G. Parton, I. H. Mather, H. Stunnenberg, K. Simons, B. Hoflack, M. Zerial, The small GTPase Rab5 functions as a regulatory factor in the early endocytic pathway. *Cell* **70**, 715–728 (1992).

25. H. Stenmark, R. G. Parton, O. Steele-Mortimer, A. Lütcke, J. Gruenberg, M. Zerial, Inhibition of Rab5 GTPase activity stimulates membrane fusion in endocytosis. *EMBO J.* **13**, 1287–1296 (1994).
26. N. C. Simon, J. T. Barbieri, Exoenzyme S ADP-ribosylates Rab5 effector sites to uncouple intracellular trafficking. *Infect. Immun.* **82**, 21–28 (2014).
27. A. Wittinghofer, I. R. Vetter, Structure-function relationships of the G domain, a canonical switch motif. *Annu. Rev. Biochem.* **80**, 943–971 (2011).
28. M. Zerial, H. McBride, Rab proteins as membrane organizers. *Nat. Rev. Mol. Cell Biol.* **2**, 107–117 (2001).
29. R. Villaseñor, Y. Kalaidzidis, M. Zerial, Signal processing by the endosomal system. *Curr. Opin. Cell Biol.* **39**, 53–60 (2016).
30. R. S. Flannagan, G. Cosío, S. Grinstein, Antimicrobial mechanisms of phagocytes and bacterial evasion strategies. *Nat. Rev. Microbiol.* **7**, 355–366 (2009).
31. K. Ireton, L. A. Rigano, G. C. Dowd, Role of host GTPases in infection by *Listeria* monocytogenes. *Cell. Microbiol.* **16**, 1311–1320 (2014).
32. A. M. Barbieri, Q. Sha, P. Bette-Bobillo, P. D. Stahl, M. Vidal, ADP-ribosylation of Rab5 by ExoS of *Pseudomonas aeruginosa* affects endocytosis. *Infect. Immun.* **69**, 5329–5334 (2001).
33. R. Madan, G. Krishnamurthy, A. Mukhopadhyay, SopE-mediated recruitment of host Rab5 on phagosomes inhibits *Salmonella* transport to lysosomes. *Methods Mol. Biol.* **445**, 417–437 (2008).
34. H. Sarantis, D. M. Balkin, P. De Camilli, R. R. Isberg, J. H. Brumell, S. Grinstein, Yersinia entry into host cells requires Rab5-dependent dephosphorylation of PI(4,5)P_2 and membrane scission. *Cell Host Microbe* **11**, 117–128 (2012).
35. A. G. Rodriguez-Gabin, M. Cammer, G. Almazan, M. Charron, J. N. Larocca, Role of rRAB22b, an oligodendrocyte protein, in regulation of transport of vesicles from trans Golgi to endocytic compartments. *J. Neurosci. Res.* **66**, 1149–1160 (2001).
36. M. S. Dhar, J. S. Virdi, Strategies used by *Yersinia enterocolitica* to evade killing by the host: Thinking beyond Yops. *Microbes Infect.* **16**, 87–95 (2014).
37. J. Ryckaert, P. Bossier, K. D'Herde, A. Diez-Fraile, P. Sorgeloos, F. Haesebrouck, F. Pasmans, Persistence of *Yersinia ruckeri* in trout macrophages. *Fish Shellfish Immunol.* **29**, 648–655 (2010).
38. A. Sulakvelidze, *Yersiniae* other than *Y. enterocolitica*, *Y. pseudotuberculosis*, and *Y. pestis*: The ignored species. *Microbes Infect.* **2**, 497–513 (2000).
39. A. A. Ribeiro, M. A. Azcarate-Peril, M. B. Cadenas, N. Butz, B. J. Paster, T. Chen, E. Bair, R. R. Arnold, The oral bacterial microbiome of occlusal surfaces in children and its association with diet and caries. *PLOS ONE* **12**, e0180621 (2017).
40. M. R. Hurst, S. A. Jones, T. Binglin, L. A. Harper, T. A. Jackson, T. R. Glare, The main virulence determinant of *Yersinia entomophaga* MH96 is a broad-host-range toxin complex active against insects. *J. Bacteriol.* **193**, 1966–1980 (2011).
41. T. M. Fuchs, G. Bresolin, L. Marcinowski, J. Schachtner, S. Scherer, Insecticidal genes of *Yersinia spp.*: Taxonomical distribution, contribution to toxicity towards *Manduca sexta* and *Galleria mellonella*, and evolution. *BMC Microbiol.* **8**, 214 (2008).
42. J. Cavallius, W. C. Merrick, Site-directed mutagenesis of yeast eEF1A. Viable mutants with altered nucleotide specificity. *J. Biol. Chem.* **273**, 28752–28758 (1998).
43. Y. Qi, Z. Liang, Z. Wang, G. Lu, G. Li, Determination of Rab5 activity in the cell by effector pull-down assay. *Methods Mol. Biol.* **1298**, 259–270 (2015).
44. P. R. Evans, G. N. Murshudov, How good are my data and what is the resolution? *Acta Crystallogr. D Biol. Crystallogr.* **69**, 1204–1214 (2013).
45. P. D. Adams, P. V. Afonine, G. Bunkóczi, V. B. Chen, I. W. Davis, N. Echols, J. J. Headd, L.-W. Hung, G. J. Kapral, R. W. Grosse-Kunstleve, A. J. McCoy, N. W. Moriarty, R. Oeffner, R. J. Read, D. C. Richardson, J. S. Richardson, T. C. Terwilliger, P. H. Zwart, PHENIX: A comprehensive Python-based system for macromolecular structure solution. *Acta Crystallogr. D Biol. Crystallogr.* **66**, 213–221 (2010).
46. P. Emsley, B. Lohkamp, W. G. Scott, K. Cowtan, Features and development of Coot. *Acta Crystallogr. D Biol. Crystallogr.* **66**, 486–501 (2010).
47. A. J. McCoy, Solving structures of protein complexes by molecular replacement with Phaser. *Acta Crystallogr. D Biol. Crystallogr.* **63**, 32–41 (2007).
48. G. Bricogne, E. Blanc, M. Brandl, C. Flensburg, P. Keller, P. Paciorek, P. Roversi, A. Sharff, O. Smart, C. Vonrhein, T. Womack, *BUSTER version 2.10.2* (Cambridge, United Kingdom: Global Phasing Ltd., 2011).
49. L. Holm, L. M. Laakso, Dali server update. *Nucleic Acids Res.* **44**, W351–W355 (2016).

Acknowledgments: We thank O. Wunderlich and V. Kreiner for excellent technical assistance and Y. Belyi for the support in yeast work. **Funding:** This study was supported by the Deutsche Forschungsgemeinschaft (DFG) AK 784 6/16-4 (to K.A.), CRC 746 (to K.A. and C.H.), and the DFG under Germany's Excellence Strategy (CIBSS–EXC-785 2189–Project ID 390939984 to C.H.).
Author contributions: G.S.O. designed and performed the experiments, analyzed the data, and wrote the paper; C.W., X.B., W.-C.K., and C.H. performed the structure determination and analysis; C.W. and C.H. contributed to the writing of the manuscript; B.S. and P.J.K.A. designed and performed the experiments and analyzed the data; P.P., T.J., and C.S. designed the experiments and analyzed the data; A.S. performed the MS analyses and analyzed the data; and K.A. supervised the study, designed the experiments, analyzed the data, and wrote the manuscript. All authors discussed the results and commented on the manuscript. **Competing interests:** The authors declare that they have no competing interests. **Data and materials availability:** All data needed to evaluate the conclusions in the paper are present in the paper and/or the Supplementary Materials. Additional data related to this paper may be requested from the authors.

Submitted 21 August 2019
Accepted 17 December 2019
Published 11 March 2020
10.1126/sciadv.aaz2094

Citation: G. S. Ost, C. Wirth, X. Bogdanović, W.-C. Kao, B. Schorch, P. J. K. Aktories, P. Papatheodorou, C. Schwan, A. Schlosser, T. Jank, C. Hunte, K. Aktories, Inverse control of Rab proteins by *Yersinia* ADP-ribosyltransferase and glycosyltransferase related to clostridial glucosylating toxins. *Sci. Adv.* **6**, eaaz2094 (2020).